Vanadium isotope fractionation of alkali basalts during mantle melting

Zhenwu Chen[1], Xin Ding[1, 2*], Ekaterina S. Kiseeva[3], Xiaobao Lin[4], Jian Huang[1, 2], Fang Huang[1, 2]

[1]CAS Key Laboratory of Crust-Mantle Materials and Environments, School of Earth and Space Sciences, University of Science and Technology of China, Hefei 230026, China

[2]CAS Center for Excellence in Comparative Planetology, University of Science and Technology of China, Hefei 230026

[3]School of Biological, Earth and Environmental Sciences, University College Cork, Distillery Fields, North Mall, Cork, T23 N73K, Ireland

[4]Department of Geology, University of Illinois at Urbana-Champaign, 1301 W. Green Street, Urbana, IL 61801, USA

[*] Correspondence to: xinding@ustc.edu.cn

Abstract

It is well known that vanadium (V) is redox-sensitive during magmatism, but whether V isotopes can be used as a mantle oxygen fugacity (fO_2) sensor remains controversial. Before using V isotopes as a redox proxy, it is crucial to understand the fractionation behavior and controlling factors of V isotopes during mantle melting. This study reports high-precision V isotopic data for alkali basalts with high fO_2 in eastern China, which were derived from carbonated mantle by a low degree of partial melting. Our results show that their $\delta^{51}V$ values (-0.85‰ to -0.61‰) are higher than those of bulk silicate Earth (BSE) and mid-ocean ridge basalts (MORBs). Chemical alteration, crustal contamination or fractional crystallization negligibly affect the $\delta^{51}V$ values of alkali basalts. Although subducted carbonates are involved in the mantle source region under eastern China, mass balance calculations show that the incorporation of carbonates did not significantly increase the $\delta^{51}V$ values of alkali basalts. In contrast, the observed high $\delta^{51}V$ values probably reflect that mantle melting controls the V isotopic compositions of mantle-derived melts. The relative abundances of V^{5+}, V^{4+} and V^{3+} in silicate melt are influenced by the variation of fO_2 and/or the degree of partial melting. Basaltic melts tend to be enriched in V with high valence at the condition of high fO_2 during mantle melting, which contributes to the enrichment of ^{51}V in alkali basalts because of the affinity of high valence V and ^{51}V. Because mantle minerals are overall more compatible of V with low valence, the valence states of V in silicate melt tend to be higher at low degree of partial melting, resulting in more significant fractionation of V isotopes. Therefore, this study validates discernable V isotope fractionation during partial melting of the mantle and examines the potential of using V isotopes to trace the redox state of magmatic systems.

1. Introduction

Vanadium exhibits moderate incompatibility during mantle melting (McDonough and Sun, 1995). The valence states of V (V^{5+}, V^{4+}, V^{3+}, V^{2+}, V^{0}) vary over a wide range of redox conditions in the inner solar system, making it a potential indicator of mantle fO_2 (Mallmann and O'Neill, 2009). For example, the speciation of V in planetary basaltic glasses has been used as a proxy for the oxidation state of Earth, Moon, and Mars (Sutton et al.,2005; Karner et al., 2006). The ratios of V to redox-insensitive homovalent elements with similar compatibility (e.g., Sc, Yb) during mantle melting were applied to constrain the fO_2 in the subarc mantle and oceanic mantle (Li and Lee, 2004; Laubier et al., 2014).

Vanadium has two stable isotopes, ^{51}V (99.76%) and ^{50}V (0.24%). Vanadium isotopic compositions are reported as $\delta^{51}V = [(^{51}V/^{50}V)_{sample}/(^{51}V/^{50}V)_{AA}-1] \times 1000$ (‰), where AA (Alfa Aesar) is the international V isotope reference material (Nielsen et al., 2011). Analytical technique advances using multi-collector inductively coupled plasma mass spectrometry (MC-ICPMS) make it possible to explore geochemical processes using high-precision V isotopic data (e.g., Nielsen et al., 2011; Prytulak et al., 2011; Schuth et al., 2017). Theoretical and experimental studies have shown that changes in V oxidation states are related to isotope fractionation. The stronger bonds formed in higher oxidation states and lower coordination environments favor heavier isotopes. As a result, V isotopes have the potential to constrain the fO_2 of magmatic systems. However, Anatahan lavas (~ ΔFMQ +2, De Moor et al., 2005) and Hekla lavas (close to FMQ, Moune et al., 2007; Shorttle et al., 2015) with different fO_2 have similar V isotopic compositions. Prytulak et al. (2017) proposed that V isotopic variations due to the different fO_2 are so subtle that they could be overprinted by fractionation induced by bonding environments. Novella et al. (2020) found

68 that V isotopes of primitive basalts along the Reykjanes Ridge are insensitive to the fO_2
69 variation of ΔFMQ -0.32 to ΔFMQ +0.06.

70 The fO_2 of mantle-derived magma varies over eight orders of magnitude from MORB
71 to minette (Carmichael, 1991). As the most abundant mantle-derived magma, the fO_2 of
72 MORB approaches the FMQ buffer (ΔFMQ +0.1, Berry et al., 2018). MORBs from the
73 Pacific, Atlantic, and Indian spreading centers have been studied to show globally
74 homogeneous fO_2 (Bézos and Humler, 2005). However, the magmatic fO_2 recorded by
75 carbonatites and associated alkaline rocks are ΔFMQ +1.4 and ΔFMQ +1.3, respectively
76 (Braunger et al., 2020), while the alkaline rocks not associated with carbonatites are formed
77 in relatively reduced environments (ΔFMQ -1.1, Braunger et al., 2020). Basanites are
78 alkali-rich mantle-derived melts, typically produced at a low degree of partial melting (~1%
79 or less), and some of them even crystallized sulfate minerals, indicating fO_2 > ΔFMQ +2
80 (Carmichael and Ghiorso, 1986; Jugo, 2009). To study the sensitivity of V isotopes to
81 mantle fO_2, it would be intriguing to analyze V isotopes for mantle-derived magmas formed
82 under more oxidized conditions.

83 Cenozoic continental basalts are widely distributed throughout eastern China, with
84 chemical compositions ranging from low-Si nephelinite, basanite, and alkali olivine basalt
85 to high-Si tholeiite (Zhou and Armstrong, 1982; Xu et al., 2005). Based on the V olivine-
86 whole rock distribution coefficients, Hong et al. (2020) estimated that the fO_2 of alkali
87 basalts in eastern China approaches ΔFMQ +1.6. He et al. (2019) studied the Fe isotopes
88 and $Fe^{3+}/\sum Fe$ ratios of alkali basalts from eastern China and found that the fO_2 of alkali
89 basalts is as high as ΔFMQ +4.1, and the $Fe^{3+}/\sum Fe$ ratio in the mantle source may be as

high as 0.15. Therefore, alkali basalts provide a good opportunity to investigate the sensitivity of V isotopes to mantle fO_2.

We measured V and Fe isotopic compositions and $Fe^{3+}/\sum Fe$ ratios for alkali basalts from eastern China, which are generally produced by a low degree of mantle melting (< ~5%, Tang et al., 2006; Huang et al., 2015; Liu et al., 2016). These alkali basalts are characterized by low $\delta^{26}Mg$ and high $\delta^{66}Zn$ values compared with mantle peridotites, leading a number of researchers to propose that the mantle source is enriched in subducted carbonates (Yang et al., 2012; Huang et al., 2015; Liu et al., 2016; Li et al., 2017). This study aims to evaluate V isotope fractionation during mantle melting and assess the sensitivity of V isotopes to mantle fO_2.

2. Geological settings and samples

Eastern China consists of the Xing-Meng Block, North China Block (NCB) and South China Block (SCB) on the eastern edge of the Eurasian continent (Fig. 1). Widespread continental basalts are distributed in eastern China and constitute an important part of the circum-Pacific volcanic belt (Zhou and Armstrong, 1982). Most of these basalts are alkali-rich varieties, and tholeiites also exist in several locations (Xu et al., 2005). The major and trace element concentrations and radiogenic isotopic data of these alkali-rich basalts are similar to those of ocean island basalts (OIBs), which represent typical intraplate alkali lavas derived from asthenospheric mantle upwelling and decompression melting (Wang et al., 2018; Guo et al., 2020). Alkali basalts from eastern China are characterized by low $\delta^{26}Mg$ and high $\delta^{66}Zn$ values relative to mantle peridotites, which record mantle metasomatism by recycled carbonates from the western Pacific Plate (Huang et al., 2015;

Li et al., 2017). Seismic tomography results also indicate that the western Pacific Plate stagnates in the mantle transition zone under eastern China (Huang and Zhao 2006).

Twenty-eight samples were collected from several locations in eastern China (Fig. 1). The collected samples belong to alkali basalts (Fig. 2a). These alkali basalts have porphyritic structures, and their phenocrysts are composed of olivine, orthopyroxene, clinopyroxene, and plagioclase. The matrix consists of olivine, augite, plagioclase, magnetite and glass. Alkali basalts are generally fresh, and only a few samples have slight iddingsitization of olivine (Tang et al., 2006; Huang et al., 2015). The collected samples were analyzed for the V and Fe isotopic compositions. These samples (except FS-10) were also measured for $Fe^{3+}/\sum Fe$ ratios. Ten samples were previously measured for Fe isotopes, and four samples were previously measured for $Fe^{3+}/\sum Fe$ ratios by He et al. (2019). Detailed sample information, major and trace element concentrations, and Sr-Nd isotopic data can be found in Tables S1-S3.

3. Analytical Methods

3.1 V isotopes

The chemical separation and measurement protocol for V isotopes are similar to those in Wu et al. (2016). Approximately 30 to 70 mg of sample powders containing 10 μg of V were dissolved in Savillex beakers using concentrated HF + HNO_3 (3:1, v/v) and heated at 140°C on hotplate for 3 days. After evaporation, the samples were treated with HCl + HNO_3 (3:1, v/v) and HNO_3 to remove the remaining fluorides. Finally, the samples were re-dissolved in 1 ml of 1 mol/L HNO_3 for column chemistry. Vanadium was purified with AG50W-X12 (200-400 mesh) cation resin and AG1-X8 (200-400 mesh) anion resin. The

136 cation resin was used to remove the main matrix elements (e.g., Al, Ca, Ti, Fe, and Cr),
137 and the anion resin was used to further remove residual matrix and isobaric elements (e.g.,
138 Na, Mg, Cr). The total blank of the procedure was less than 2.5 ng, which is negligible
139 compared with the 10 μg V processed. The V yields in the total column chemistry were >
140 99%.

141 Vanadium isotopic ratios were measured by the sample-standard bracketing method
142 using a Thermo-Fisher Scientific MC-ICP-MS (Neptune Plus) at the University of Science
143 and Technology of China (USTC). The V concentration difference between the samples
144 and bracketing standard solution was adjusted to be within 10%. The sensitivity of ^{51}V was
145 ~ 200 V/ppm using a 10^{10} Ω amplifier in medium resolution mode ($M/\Delta M > 4000$) as
146 detected by Aridus II desolvator (CETAC Technologies) under dry plasma conditions. The
147 sample solution introduced into the instrument had V concentration of ~ 800 ppb and the
148 detected signal of ~ 0.4 V on mass ^{50}V using a 10^{11} Ω amplifier. To correct the isobaric
149 interference of ^{50}Cr and ^{50}Ti on ^{50}V, ^{53}Cr and ^{49}Ti were simultaneously collected in L4 and
150 H1 Faraday cups, respectively. Based on the average $\delta^{51}V$ values of three in-house
151 standards BDH, NIST-3165 and USTC-V of -1.23 ± 0.08‰ (2SD, n = 1265), 0.70 ± 0.08‰
152 (2SD, n = 650) and 0.07‰ ± 0.09‰ (2SD, n = 376), respectively, the long-term
153 reproducibility of V isotopes analysis was better than 0.09‰ (2SD). The $\delta^{51}V$ values of
154 USGS basalt standards (BIR-1: -0.94 ± 0.04‰, 2SD; BCR-2: -0.80 ± 0.05‰, 2SD)
155 analyzed in this study are identical to the literature values (BIR-1: -0.92 ± 0.09‰; BCR-2:
156 -0.78 ± 0.08‰) (Wu et al., 2016). In addition, repeated digestion and measurements of
157 three samples (13PMS2, 13PMS6, 10FS10) show excellent reproducibility within the
158 analytical errors of 0.09‰.

3.2 Fe isotopes

The sample dissolution and column chemistry for Fe isotopes are briefly described below using procedures similar to those in Huang et al. (2011). Sample powders containing ~ 100 μg of Fe were dissolved in Savillex beakers by a mixture of concentrated HF + HNO_3 (3:1, v/v). After evaporation, concentrated HCl was used to remove residual fluorides. Finally, the samples were dissolved in 0.5 ml of 6 mol/L HCl for column chemistry. The total blank of the procedure was less than 35 ng, which is negligible compared with the 100 μg Fe processed.

Iron isotopic ratios were measured by the standard bracketing method at USTC. Iron isotopic compositions are reported as $\delta^{56}Fe = [(^{56}Fe/^{54}Fe)_{sample}/(^{56}Fe/^{54}Fe)_{IRMM\text{-}014}\text{-}1] \times 1000$ (‰), where IRMM-014 is the international Fe isotope reference material (Williams et al., 2005). Based on the average $\delta^{56}Fe$ values of two in-house standards UIFe and GSB that were 0.69 ± 0.05‰ (2SD, n = 1219) and 0.72 ± 0.05‰ (2SD, n = 771), respectively, the long-term reproducibility of Fe isotopes analysis was better than 0.05‰ (2SD). The $\delta^{56}Fe$ values of three USGS basalt standards (BIR-1: 0.06‰ ± 0.03‰, 2SD; BCR-2: 0.07‰ ± 0.04‰, 2SD; BHVO-2: 0.11‰ ± 0.04‰, 2SD) obtained in this study are identical to the literature values (BIR-1: 0.05 ± 0.02‰; BCR-2: 0.09 ± 0.01‰; BHVO-2: 0.11‰ ± 0.01‰) (Craddock and Dauphas, 2011). In addition, replicates of four samples (13PMS1, 13PMS7, FS-2, and FS-33) by digestion of separate rock powders show excellent reproducibility within the analytical errors of 0.05‰. These results confirm the reliability of the Fe isotopic compositions.

3.3 Mössbauer spectra analysis of $Fe^{3+}/\sum Fe$ ratios

The $Fe^{3+}/\sum Fe$ ratios of alkali basalts were measured at Guangzhou Institute of Geochemistry, Chinese Academy of Science (GIGCAS). Approximately 50 mg of each sample was uniformly placed in the holder and measured at room temperature (298 K). Mössbauer spectra were collected in transmission mode using a Silver Double Limited WSS-10 spectrometer. A ^{57}Co in the Rh matrix was used as the Mössbauer source. The velocity drive transducer operates in a triangular waveform mode over an energy range of ± 15 mm/s. All spectra were calibrated against 7 μm α-Fe foil and fit using MossWinn software. The spectra were deconvoluted based on the least square fitting of the Lorentzian line-shaped profile, and the subspectra assigned to different phases were classified according to their hyperfine parameters [i.e., isomer (IS), quadrupole splitting (QS), and magnetic hyperfine field (BHF)]. The proportion of each phase was determined by the area of its corresponding subspectrum.

4. Results

Vanadium and iron isotopic data of alkali basalts, together with the whole rock $Fe^{3+}/\sum Fe$ ratios are presented in Table 1. The samples display an overall range of $\delta^{51}V$ values from -0.85‰ to -0.61‰, with an average value of -0.72 ± 0.11‰ (2SD, n = 28). As shown in Fig.3, the V isotopic compositions of alkali basalts are higher than those of MORBs (-0.96‰ to -0.76‰, average -0.84 ± 0.10‰, 2SD, n = 22, Wu et al., 2018), OIBs (-1.00‰ to -0.63‰, average -0.81 ± 0.16‰, 2SD, n = 8, Ding et al., 2020), komatiites (-0.95‰ to -0.86‰, average -0.91 ± 0.05‰, 2SD, n = 10, Qi et al., 2019) and the BSE (-0.91‰ to -0.86‰, average -0.91 ± 0.09‰, 2SD, n = 18, Qi et al., 2019; Nielsen et al.,

2020). The $\delta^{56}Fe$ values for the alkali basalts range from 0.11‰ to 0.26‰, with an average value of 0.20 ± 0.09‰ (2SD, n = 28). These values are systematically higher than those of MORBs (0.07‰ to 0.14‰, Teng et al., 2013) and BSE (0.02 ± 0.03‰, Weyer and Ionov, 2007). The $\delta^{56}Fe$ and $\delta^{51}V$ values of alkali basalts are both negatively correlated with SiO_2 contents (Figs. 2b and 2c). The alkali basalts have much higher $Fe^{3+}/\sum Fe$ ratios than MORBs (~ 0.10, Berry et al., 2018), varying from 0.21 to 0.64.

5. Discussion

5.1 The effects of alteration, contamination, and magma differentiation

To understand the elevation in $\delta^{51}V$, we must evaluate whether the V isotopic compositions of alkali basalts were influenced by alteration and magma differentiation. The loss of ignition of alkali basalts ranges from 0.10 wt.% to 4.94 wt.%, indicating that few samples may have undergone alteration. The observations of thin sections indicate that most samples are fresh, but olivine phenocrysts in several samples have slight iddingsitization (Tang et al., 2006; Huang et al., 2015). Because V is highly incompatible in olivine (Mallmann and O'Neill, 2009), iddingsitization would not have significantly affected the V isotopic compositions of bulk rocks. Prytulak et al. (2013) found that serpentinization of olivine did not cause V isotope fractionation. In addition, V is relatively immobile during alteration. The $\delta^{51}V$ measurements of mafic oceanic crust and the weathering profile of gabbro show that the alteration and weathering did not cause significant V isotope fractionation (Prytulak et al., 2013; Qi et al., 2022). Therefore, weathering and alteration are not responsible for the enrichment of ^{51}V in alkali basalts.

When continental basalt passes through thick continental crust before erupting, crustal contamination and fractional crystallization are likely to occur during magmatic evolution. The Nb/U (28-48) and Ce/Pb (17-34) ratios of alkali basalts are similar to those of OIBs (Nb/U = 47 ± 10, Ce/Pb = 25 ± 5, Hofmann et al., 1986) and clearly higher than those of continental crust (Nb/U = 6.2, Ce/Pb = 4, Rudnick and Gao, 2003), which rules out the possibility of significant crustal contamination. Most alkali basalts have depleted Sr and Nd isotopic compositions with $^{87}Sr/^{86}Sr(i)$ from 0.70331 to 0.70426 and $\varepsilon Nd(t)$ from 0.05 to 5.90, which indicate a limited degree of crustal contamination (Tang et al., 2006; Huang et al., 2015; Liu et al., 2016). The $\delta^{51}V$ of continental crust varies from -0.80‰ to -0.50‰ (Wu et al., 2020); therefore, we choose -0.65‰ as the V isotopic composition of the continental crust to simulate crustal contamination. The average continental crust V content of 138 ppm (Rudnick and Gao, 2003) is selected as the crustal endmember. The V content and isotopic composition of primary alkali basaltic magma are set to 200 ppm and -0.86‰, respectively. The simulation results indicate that the contribution of ~70% crust is required to produce alkali basalts with the V isotopic composition of -0.72‰. Therefore, crustal contamination cannot explain the elevation of $\delta^{51}V$ values of alkali basalts.

Tang et al. (2006) and Huang et al. (2015) suggested that the geochemical compositions of alkali basalts were close to that of primary magma without obvious fractional crystallization. The phenocrysts of alkali basalts mainly consist of olivine, pyroxene and plagioclase. Vanadium is an incompatible element in olivine and plagioclase (Bougault and Hekinian, 1974; Zanetti et al., 2004), and the V isotopic compositions of residual melts tend to be constant during early magma differentiation. The partition coefficient of V between pyroxene and melt ranges from 1.8 to 3.1 (Hart and Dunn, 1993; Hauri et al.,

1994). However, studies of Anatahan and Hekla lavas show that the crystallization of pyroxene does not affect the V isotopic compositions of the residual melt (Prytulak et al., 2017). The V isotopic compositions are invariant during the crystallization stage of pyroxene in the magmatic system of the mid-ocean ridge environment (Wu et al., 2018). In addition, the $\delta^{51}V$ values of alkali basalts are negatively correlated with SiO_2 contents (Fig. 2c), which is contrary to the predicted trend of magma differentiation (Prytulak et al., 2017; Wu et al., 2018; Ding et al., 2020). Therefore, we conclude that the heavier V isotopic compositions of alkali basalts cannot be the result of magma differentiation.

5.2 $\delta^{51}V$ variations in alkali basalts do not reflect source signatures

Previous studies have emphasized that the mantle sources in eastern China are heterogeneous, which is manifested by the incorporation of recycled carbonates from the subducting Pacific Plate (Zeng et al., 2010; Li et al., 2017). The geochemical signature for addition of carbonates is evidenced by trace element ratios and Mg-Zn isotopic compositions. It is thus necessary to discuss whether the mantle heterogeneity leads to V isotopic variations in alkali basalts. Alkali basalts from eastern China have Zr/Hf ratios higher than chondrites and significant negative Zr, Hf and Ti anomalies, indicating the existence of carbonate metasomatism in the mantle source (Huang et al., 2015; Liu et al., 2016). Compared with the Mg and Zn isotopic compositions of mantle peridotites ($\delta^{26}Mg$ = -0.25‰ ± 0.07‰, $\delta^{66}Zn$ = 0.18‰ ± 0.05‰, Teng et al., 2010; Wang et al., 2017), carbonates have lower $\delta^{26}Mg$ (-2.52‰ to -0.51‰, Higgins and Schrag, 2010) and higher $\delta^{66}Zn$ values (0.91 ± 0.05‰, Pichat et al., 2003). The $\delta^{26}Mg$ (-0.57‰ to -0.30‰) and $\delta^{66}Zn$

(0.30‰ to 0.58‰) values of alkali basalts reflect the mixing of the end-members (Yang et al., 2012; Huang et al., 2015; Liu et al., 2016).

Although carbonates have V isotopic compositions ($\delta^{51}V$ = -0.54‰ to -0.79‰, Dong et al., 2021) heavier than those of mantle peridotites (-0.91‰ to -0.86‰, Qi et al., 2019; Nielsen et al., 2020), the V content in carbonates (< 5 ppm; Kilias et al., 2006; Li et al., 2014; Dong et al., 2021) is much lower than that in mantle (~ 82 ppm, McDonough and Sun, 1995). We use mass balance calculations to evaluate the effect of carbonate incorporation on the V isotopic composition of the mantle source. The V content and V isotopic composition of carbonates are set at 5 ppm and -0.54‰, and the values of mantle are set at 82 ppm and -0.86‰. Even if the proportion of carbonates reaches 50%, the calculated V isotopic composition of the mantle is estimated to be -0.84‰ (Fig. 4), which is definitely lower than the average $\delta^{51}V$ value of alkali basalts (-0.72‰). Therefore, the incorporation of carbonate is insufficient to increase the V isotopic composition of the mantle source of alkali basalts.

Most alkali basalts from NCB have Fe/Mn ratios greater than 65, which is generally high than those of from SCB (Fig. 5a). Because Fe is compatible in olivine and Mn is preferentially partitioned into clinopyroxene and garnet, the $D_{Fe}^{bulk/melts}$ value of pyroxenite tends to be lower than that of peridotite, while the $D_{Mn}^{bulk/melts}$ of pyroxenite may be higher than that of peridotite (Sobolev et al., 2007; Le Roux et al., 2010). In this case, the higher Fe/Mn ratios of alkali basalts from NCB suggest a significant contribution from pyroxenite melting. The alkali basalts from SCB, which possess lower Fe/Mn ratios similar to that of MORB, are likely derived from peridotite mantle. Based on the reported values of fertile and strongly melt depleted peridotites by Qi et al. (2019), the $\delta^{51}V$ of peridotite mantle is

estimated to be between -0.95‰ to -0.85‰. However, the V isotopic composition for pyroxenite source has not been studied. Considering that the $\delta^{51}V$ values of the NCB alkali basalts (-0.85‰ to -0.67‰) containing pyroxenite melting contributions are slightly lighter than those of the SCB alkali basalts (-0.75‰ to -0.61‰) from peridotite mantle, the heavier V isotopic compositions of alkali basalts than that of MORB and BSE should not be the characteristic of pyroxenite source. Consequently, the $\delta^{51}V$ variations in alkali basalts do not reflect source signatures.

5.3 V isotope fractionation during mantle partial melting

Vanadium isotope fractionation associated with mantle partial melting appears to be the most likely mechanism for explaining the observed heavier V isotopic compositions in alkali basalts. Based on the mass-balance, the V isotopic compositions of mantle source $\left(\frac{^{51}V}{^{50}V}\right)_0$ and silicate melt $\left(\frac{^{51}V}{^{50}V}\right)_m$ can be summarized in the following equations

$$\left(\frac{^{51}V}{^{50}V}\right)_0 = \left(\frac{^{51}V^{3+}}{^{50}V^{3+}}\right)_0 * \frac{1+\alpha_{V^{4+}/V^{3+}} * \left(\frac{V^{4+}}{V^{3+}}\right)_0 + \alpha_{V^{5+}/V^{3+}} * \left(\frac{V^{5+}}{V^{3+}}\right)_0}{1+\left(\frac{V^{4+}}{V^{3+}}\right)_0 + \left(\frac{V^{5+}}{V^{3+}}\right)_0} \quad (1)$$

$$\left(\frac{^{51}V}{^{50}V}\right)_m = \left(\frac{^{51}V^{3+}}{^{50}V^{3+}}\right)_m * \frac{1+\alpha_{V^{4+}/V^{3+}} * \left(\frac{V^{4+}}{V^{3+}}\right)_m + \alpha_{V^{5+}/V^{3+}} * \left(\frac{V^{5+}}{V^{3+}}\right)_m}{1+\left(\frac{V^{4+}}{V^{3+}}\right)_m + \left(\frac{V^{5+}}{V^{3+}}\right)_m} \quad (2)$$

where subscripts 0 and m refer to mantle source and silicate melt, respectively. The $\alpha_{V^{4+}/V^{3+}}$ and $\alpha_{V^{5+}/V^{3+}}$ are isotope fractionation factors between V^{4+} and V^{3+}, V^{5+} and V^{3+}, respectively. $\left(\frac{V^{4+}}{V^{3+}}\right)$ and $\left(\frac{V^{5+}}{V^{3+}}\right)$ stand for the ratio of V^{4+}/V^{3+} and the ratio of V^{5+}/V^{3+}.

313 $\left(\frac{^{51}V^{n+}}{^{50}V^{n+}}\right)$ stands for V isotopic composition of a specific valence state, where n = 3. The
314 derivation for equations (1) and (2) can be found in the supplemental materials. For a given
315 mantle source with certain mineral assemblage, the proportion of V content in different
316 valence states is fixed. However, the relative abundances of V^{5+}, V^{4+} and V^{3+} in silicate
317 melt are influenced by the variation of fO_2 and/or the degree of partial melting. The isotope
318 fractionation ($\Delta^{51}V_{m-0}$) as represented by the difference between mantle source and silicate
319 melt is therefore changed with the variation of fO_2 and the degree of partial melting.
320
321 5.3.1 Effect of oxygen fugacity
322 Because fO_2 controls the valence states of V, the abundance of V with different valence
323 state in silicate melt varies by following the redox equations (3) and (4). The V valence
324 states in silicate melt tend to be higher at the condition of high fO_2. Heavy isotopes are
325 theoretically enriched in low coordination and high valence bonding environments
326 (Bigeleisen and Mayer, 1947; Urey, 1947; Schauble, 2004). Therefore, the silicate melt
327 under high fO_2 prefers to have more ^{51}V.

328 $$V^{3+}O_{1.5}+\frac{1}{4}O_2=V^{4+}O_2 \quad (3)$$

329 $$V^{4+}O_2+\frac{1}{4}O_2=V^{5+}O_{2.5} \quad (4)$$

330 Here we provide an approach to quantitively link fO_2 and V isotopic compositions.
331 First, the valance state of V controlled by fO_2 is determined by using the method in Toplis
332 and Corgne (2002). Second, vanadium isotope fractionation depends on the variation of V
333 valance states (Wu et al., 2015). Details of the simulation can be found in supplemental
334 materials. According to the reported $\delta^{51}V$ values, our simulations yield an average ΔFMQ

of +0.6 for MORB, ΔFMQ of +1.5 for Hawaiian OIB and ΔFMQ of +2.0 for primary arc basalts in Marianas. The estimated values are consistent with the published data in the previous studies (Ballhaus, 1993; Evans et al., 2012; Brounce et al., 2014; Greaney et al., 2017; Berry et al., 2018). By using the average $\delta^{51}V$ value of alkali basalts from eastern China, we further estimate the fO_2 to be ΔFMQ ~ +3.7 that is substantially higher than the estimates for MORB, OIB and primary arc lavas (Fig. 6a). In other words, our simulation reveals a positive correlation between fO_2 and V isotopic compositions. For Reykjanes Ridge with ΔFMQ of -0.32 to +0.06, the basalts have $\delta^{51}V$ value ranging from -1.09‰ to -0.86‰ (Novella et al., 2020). In contrast, the elevated V isotopic values up to -0.61‰ are observed in alkali basalts from eastern China under the condition of high fO_2.

Similar to V, Fe has multiple valence states and the valence state of Fe vary as a function of fO_2. Given that Fe^{3+} usually has higher $\delta^{56}Fe$ than Fe^{2+}, silicate melt prefers to enrich heavy Fe isotope relative to the mantle source during mantle partial melting. The alkali basalts have $Fe^{3+}/\sum Fe$ ratios up to 0.64, which is consistent with the data reported by He et al. (2019), indicating that silicate melt was enriched in Fe^{3+} in the formation under high fO_2 condition. As shown in Fig. 5b, the variations of $\delta^{51}V$ and $\delta^{56}Fe$ values are coupled for the alkali basalts from eastern China. He et al. (2019) proposed that the high $\delta^{56}Fe$ values of alkali basalts were formed under high fO_2 condition and fO_2 can be as high as ΔFMQ +4.1. The similar behaviors of V and Fe isotopes confirm the effect of fO_2 on isotope fractionation during mantle partial melting.

In terms of silicate melt derived from difference mantle source, the SCB alkali basalts have $\delta^{51}V$ values between -0.75‰ to -0.61‰ that are slightly higher than those of NCB alkali basalts (-0.85‰ to -0.67‰). He et al. (2019) suggested that SCB alkali basalts with

heavy Fe isotopes originated from a carbonated peridotite mantle, indicating the involvement of recycled carbonate. As carbonate is one of the most abundant oxidized phases at the top of oceanic plates (Dasgupta et al., 2010; Brounce et al., 2019), transport of carbonate into mantle by subduction could lead to local increase in mantle fO_2 (Rohrbach and Schmidt, 2011; Tao and Fei, 2021). Compared with NCB alkali basalts, SCB alkali basalts are likely to have a more oxidizing environment, resulting in the higher valence states of V and heavier V isotopic compositions in silicate melt during mantle partial melting.

5.3.2 Effect of the melting degree

Melting degree influences the abundance of V with different valence state in silicate melt by Eq. (5) and Eq. (6). Because of the increasing incompatibility from V^{3+}, V^{4+} to V^{5+} for mantle minerals (Mallmann and O'Neill, 2009), the valence states of V in silicate melt tend to be higher at low degree of partial melting. With the proceeding of mantle melting, the lower valence states of V released from residual mantle increases, resulting in the decrease of V valence states in silicate melt. When the degree of partial melting gradually approaches 100%, the proportions of V^{3+}, V^{4+} and V^{5+} in the bulk melt become the same as those in the mantle source. Therefore, the fractionation of V isotopes is determined by the relative abundances of V^{3+}, V^{4+}, and V^{5+} that enter the liquid phase during mantle partial melting.

$$\left(\frac{V^{4+}}{V^{3+}}\right)_m = \left(\frac{V^{4+}}{V^{3+}}\right)_0 * \frac{D^{V^{3+}} + F \times \left(1 - D^{V^{3+}}\right)}{D^{V^{4+}} + F \times \left(1 - D^{V^{4+}}\right)} \quad (5)$$

$$\left(\frac{V^{5+}}{V^{3+}}\right)_m = \left(\frac{V^{5+}}{V^{3+}}\right)_0 * \frac{D^{V^{3+}} + F \times \left(1 - D^{V^{3+}}\right)}{D^{V^{5+}} + F \times \left(1 - D^{V^{5+}}\right)} \quad (6)$$

where F is the degree of mantle partial melting; $D^{V^{3+}}$, $D^{V^{4+}}$, and $D^{V^{5+}}$ are the bulk partition coefficients of V^{3+}, V^{4+} and V^{5+} between mantle minerals and silicate melt.

Here we simulate the variation of $\delta^{51}V$ in relation to the degree of mantle partial melting. By embedding Eqs. (5) – (6) into Eqs. (1) – (2), the isotope fractionation between silicate melt and mantle source ($\Delta^{51}V_{m\text{-}0}$) and the $\delta^{51}V$ value of silicate melt can be estimated. Details of the simulation can be found in supplemental materials. As shown in Fig. 6b, the extent of V isotope fractionation gradually decreases with increasing degree of mantle partial melting. When the degree of partial melting is lower than ~ 7%, the predicted V isotopic compositions of melting products are comparable to that of observed $\delta^{51}V$ values in alkali basalts from eastern China that ranging from -0.85‰ to -0.61‰. When the melting degree increases, the V isotopic compositions of the melts become close to the $\delta^{51}V$ value of MORB that requires higher melting degree (6%-20%, Klein and Langmuir, 1987).

The $\delta^{51}V$ values of alkali basalts increase with increasing Nb/Y ratios (Fig. 5c). As Nb and Y are incompatible elements in olivine and orthopyroxene, fractional crystallization of olivine and orthopyroxene would not significantly change the Nb/Y ratios. Because Nb is more incompatible than Y during mantle melting, the Nb/Y ratios of silicate melt are mainly controlled by the degree of mantle melting. The high Nb/Y ratios of SCB alkali basalts indicate a low degree of partial melting during their formation. Huang et al. (2015) drew a similar conclusion based on the high La/Yb and Sm/Yb ratios of SCB alkali basalts, most of which were formed with a melting degree of 2%-3%. The high $\delta^{51}V$ values observed in SCB alkali basalts likely reflect enhanced V isotope fractionation at low degree

peridotite partial melting. If the SCB and NCB alkali basalts were derived from a same mantle source, the relatively low Nb/Y ratios of NCB alkali basalts indicate that its partial melting degree would be higher than that of SCB alkali basalts. However, pyroxenite is important in forming NCB alkali basalts. Although we cannot well constrain the degree of partial melting for NCB alkali basalts, the V isotopic compositions of NCB alkali basalts (-0.85‰ to -0.67‰) are heavier than that of MORB (-0.84 ± 0.10‰). We speculate that the melting degree of NCB alkali basalts should be lower than that of MORB. For SCB and NCB alkali basalts that representing the products of low degree partial melting, they show V isotope fractionation with the $\delta^{51}V$ values higher than that of MORB.

This study suggests that more significant fractionation of V isotopes occurs at lower melting degrees and/or more oxidizing conditions. As shown in Fig. 7, the ancient carbonate-bearing western Pacific Plate subducted into the mantle transition zone and released carbonate-rich melts. Because carbonate-rich melts exhibit low viscosity and high mobility (Thomson et al., 2016), they migrated upward and reacted with the overlying mantle, metasomatizing upper mantle above the mantle transition zone. The release of carbonate into the mantle sources can cause a local increase in mantle fO_2 (Rohrbach and Schmidt, 2011). The metasomatized carbonated mantle experienced low-degree melting during mantle upwelling, resulting in the formation of alkali basalts. Such alkali basalts tend to have heavier V isotopic compositions than MORBs.

6. Conclusion

High-precision V and Fe isotopic compositions and whole rock $Fe^{3+}/\sum Fe$ ratios for alkali basalts from eastern China lead us to the following conclusions:

(1) The V isotopic compositions of alkali basalts (-0.72 ± 0.11‰) are heavier than those of MORB (-0.96‰ to -0.76‰) and BSE (-0.91‰ to -0.86‰), which probably reflects the V isotope fractionation during mantle partial melting. In contrast, the effects of chemical alteration, crustal contamination or fractional crystallization on $\delta^{51}V$ of alkali basalts are limited.

(2) Subducted carbonates have been added to the mantle source region under eastern China, but the much lower V content of carbonates than mantle is insufficient to significantly elevate the V isotopic composition of alkali basalts.

(3) We find that fractionation of V isotopes is significant at a lower degree of partial melting and/or at a higher fO_2. This is consistent with the observed high $\delta^{51}V$ values for alkali basalts with high fO_2 from eastern China, which were derived from carbonated mantle by a low degree of partial melting.

Acknowledgements

We thank Yan-Jie Tang for providing the alkali basalt samples. This project was funded by the National Key R&D Program of China (2019YFA0708400) and the B-type Strategic Priority Research Program of the Chinese Academy of Sciences (Grant No. XDB41000000). We acknowledge support from NERC grant NE/L010828/1, IRC grant IRCLA/2022/2638, and the CAS Youth Innovation Promotion Association (Grant2019449). We gratefully acknowledge Yongsheng He and one anonymous reviewer for thorough and constructive reviews, and Di-Cheng Zhu for efficient editorial handling, which greatly improve the manuscript.

Figure captions

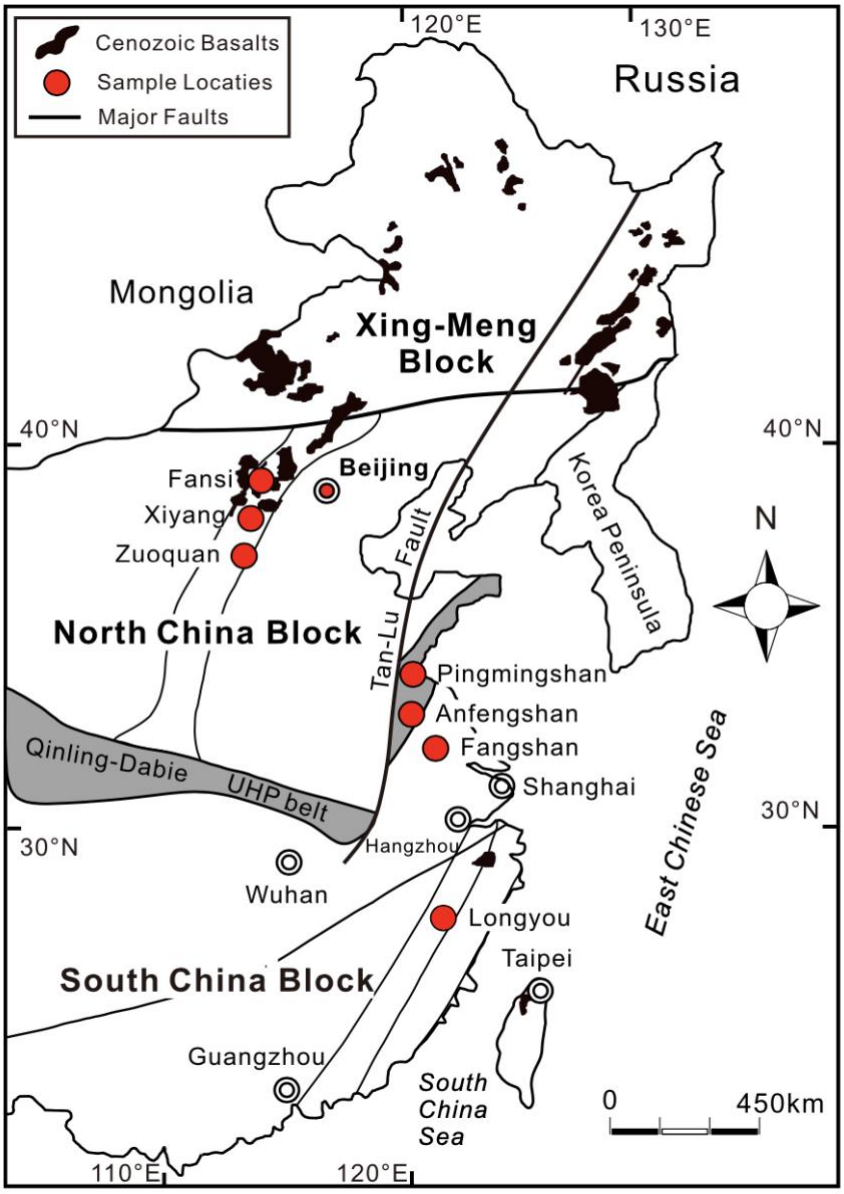

Figure 1 Simplified geological map of eastern China after Liu et al. (2016). The red filled circles represent the locations of the sampling areas.

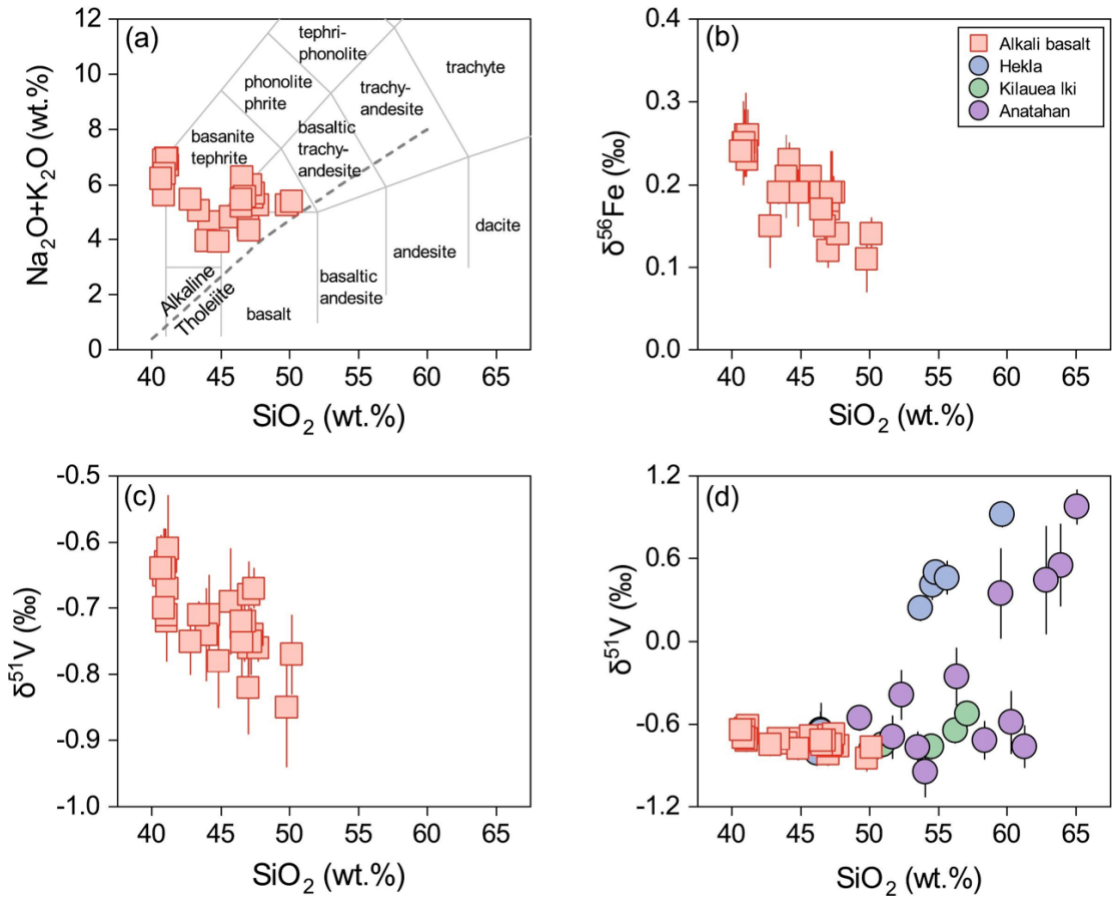

Figure 2 The contents of Na_2O+K_2O (a), $\delta^{56}Fe$ (b), and $\delta^{51}V$ (c, d) versus SiO_2 for alkali basalts from eastern China. The $\delta^{51}V$ values of Anatahan and Hekla lavas are from Prytulak et al. (2017), while those of Kilauea Iki lavas are from Ding et al. (2020).

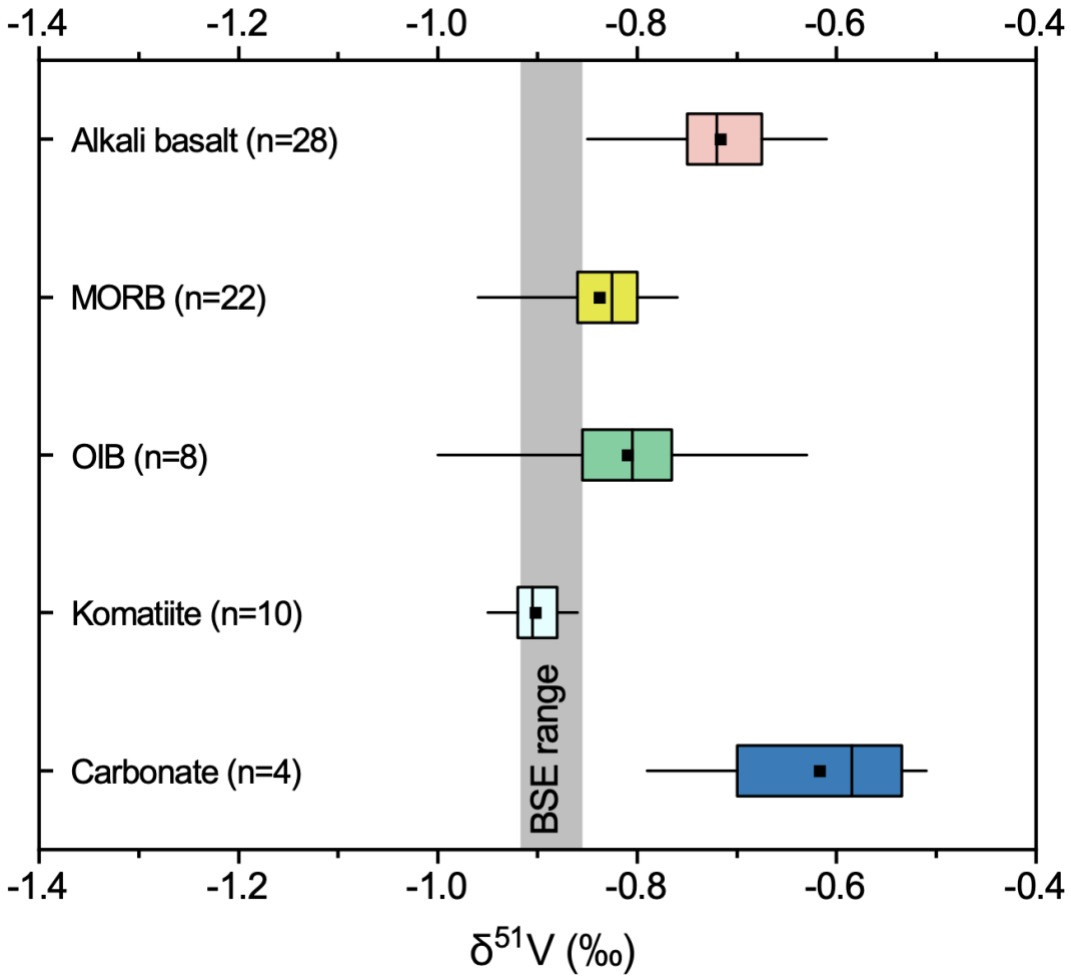

455

456 **Figure 3** Plot of V isotopic compositions of alkali basalt, MORB, OIB, komatiite and
457 carbonate. The boxes stand for the 25 to 75 percentiles, and the whiskers are 0 to 100
458 percentiles. The black squares and the vertical lines in the boxes denote the mean values
459 and the median values, respectively. The vertical gray area shows the $\delta^{51}V$ variation of the
460 BSE value (-0.91‰ to -0.86‰, Qi et al., 2019; Nielsen et al., 2020). Data sources: MORB
461 (Wu et al., 2018), OIB (Ding et al., 2020), komatiite (Qi et al., 2019) and carbonate (Dong
462 et al., 2021).

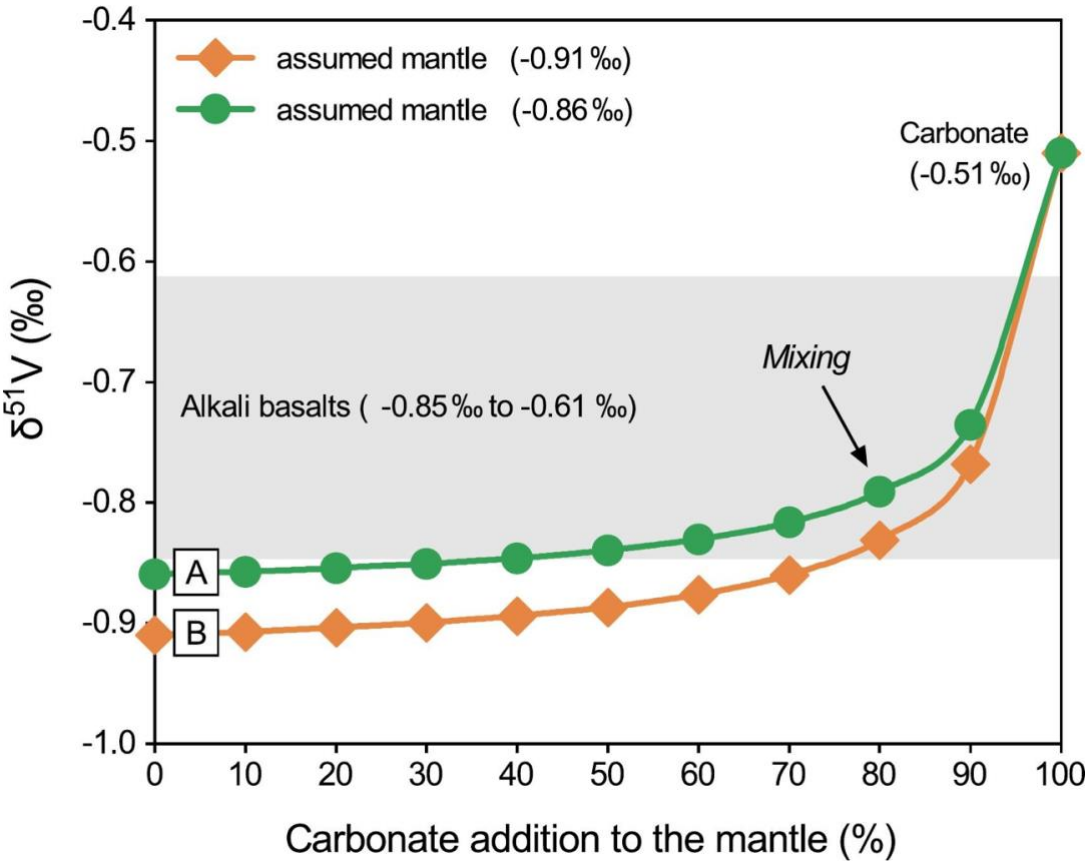

Figure 4 Two-component mixing between carbonate and mantle source. The mixing lines are marked in 10% increments. The $\delta^{51}V$ of mantle are assumed of -0.86‰ and -0.91‰, respectively. The $\delta^{51}V$ of carbonate is assumed of -0.51‰. The gray area represents the V isotopic variations of alkali basalts from eastern China.

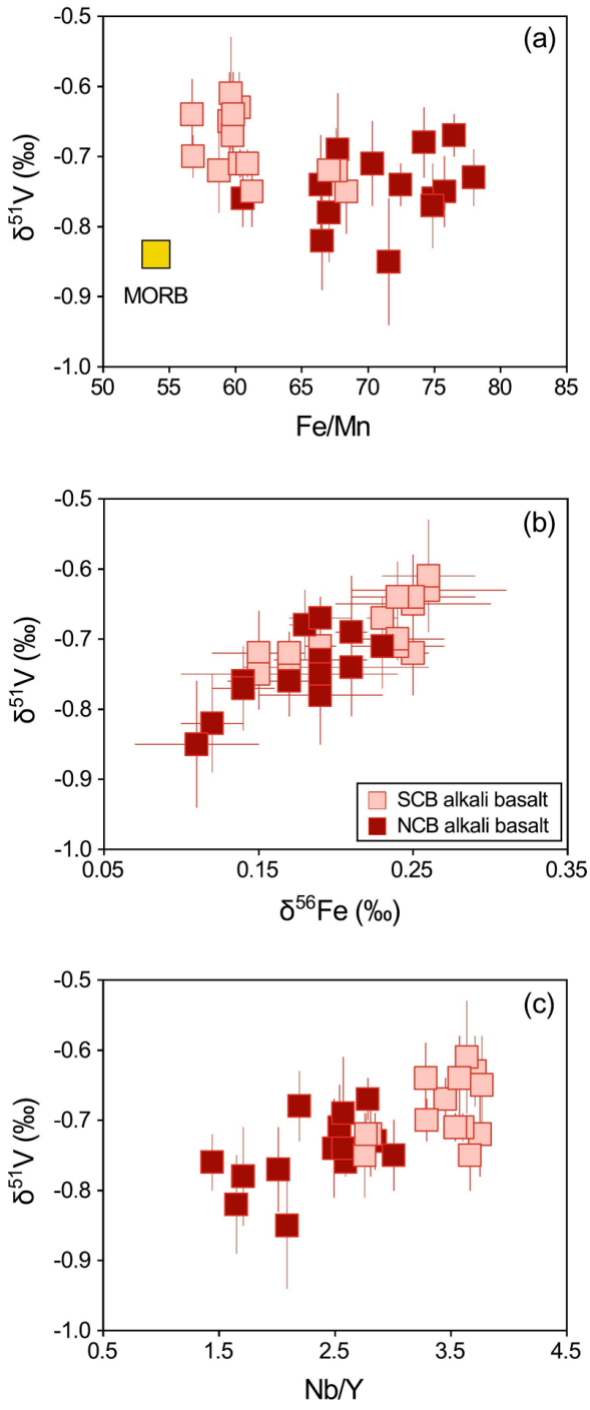

468

469 **Figure 5** Plot of (a) $\delta^{51}V$ versus Fe/Mn, (b) $\delta^{51}V$ versus $\delta^{56}Fe$, and (c) $\delta^{51}V$ versus Nb/Y

470 of alkali basalts from SCB and NCB. The Fe/Mn ratio of MORB is from Qin and Humayun

471 (2008).

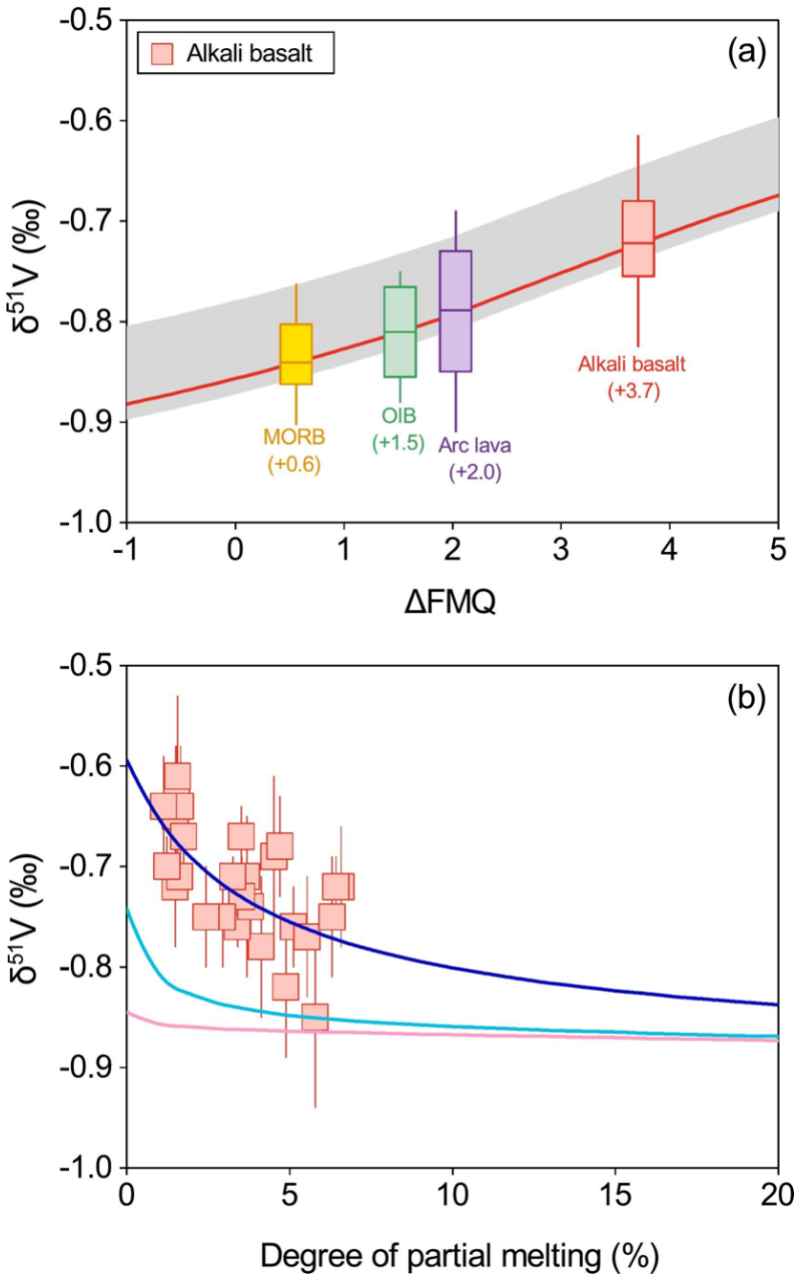

472

473 **Figure 6** Modelling of the melt $\delta^{51}V$ variation during mantle partial melting. (a) Effect of

474 fO_2 (expressed relative to the fayalite-magnetite-quartz buffer) on V isotope fractionation

475 and estimated fO_2 for MORB, OIB, arc lava and alkali basalt. The literature data of $\delta^{51}V$

476 values for MORB, OIB and arc lava are compiled in Table S4. The ends of the boxes show

477 the upper and lower quartiles, and the horizontal lines in the boxes correspond to the mean

478 values. The whiskers denote interquartile range. The upper and lower bounds of the shaded

region represent $(V^{4+}/V^{3+})_0 = 1$, $(V^{5+}/V^{3+})_0 = 0.001$ and $(V^{4+}/V^{3+})_0 = 100$, $(V^{5+}/V^{3+})_0 = 0.1$, respectively. The red curve represents $(V^{4+}/V^{3+})_0 = 10$, $(V^{5+}/V^{3+})_0 = 0.01$. (b) A comparison of measured $\delta^{51}V$ of alkali basalts with model curves showing the effect of melting degree on V isotope fractionation. Blue, cyan, and pink lines represent the V isotopic composition of melt from mantle source with $(V^{4+}/V^{3+})_0 = 1$, $(V^{5+}/V^{3+})_0 = 0.1$; $(V^{4+}/V^{3+})_0 = 1$, $(V^{5+}/V^{3+})_0 = 0.01$; and $(V^{4+}/V^{3+})_0 = 1$, $(V^{5+}/V^{3+})_0 = 0.001$, respectively. The abundance of Sm was used to estimate the melting degree of alkali basalts.

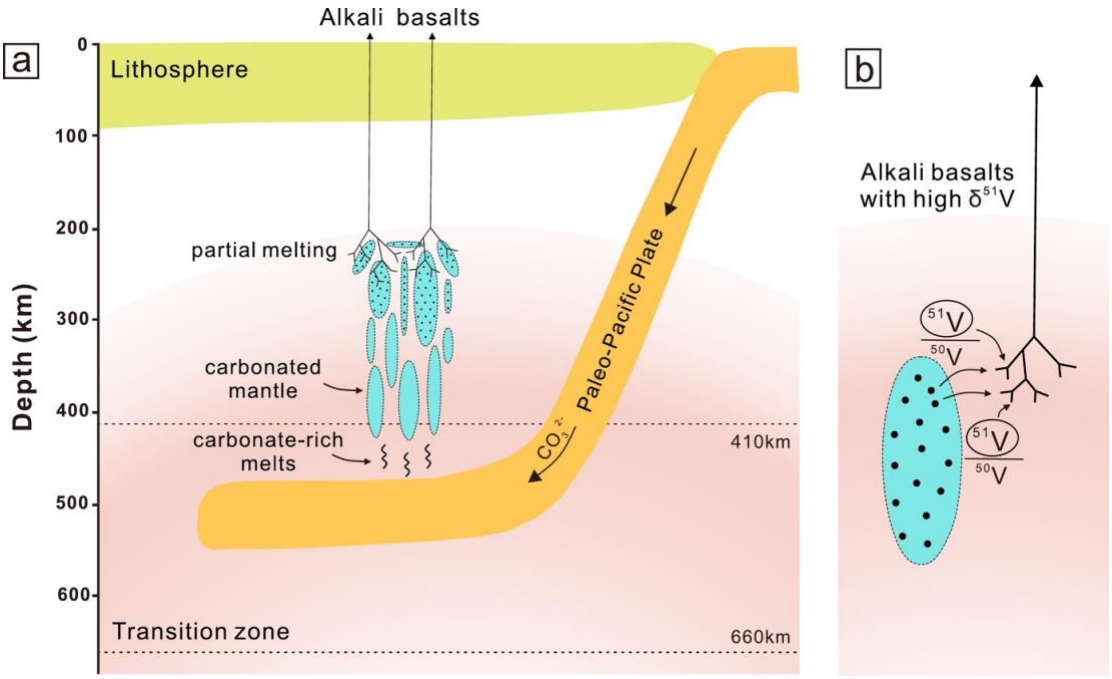

Figure 7 Schematic model of V isotope fractionation during the formation of alkali basalts. (a) The subduction of the Pacific Plate beneath the mantle transition zone produced carbonate-rich melts. Alkali basalts were produced by low-degree partial melting of carbonated mantle that experienced carbonate metasomatism. (b) During partial melting in the mantle, the heavy V isotope (^{51}V) preferentially enters the melts, resulting in high $\delta^{51}V$ values in melts.

494 # Table

Table 1 Vanadium isotopic compositions, iron isotopic compositions and whole rock $Fe^{3+}/\sum Fe$ ratios of alkali basalts from eastern China

Location	Sample	$\delta^{51}V$	2SD	$\delta^{56}Fe$	2SD	$\delta^{57}Fe$	2SD	$Fe^{3+}/\sum Fe$
Fansi	FS-2	-0.82	0.07	0.12	0.02	0.21	0.08	0.64
Fansi	FS-2*			0.14	0.02	0.22	0.05	
Fansi	FS-3	-0.76	0.04	0.17	0.02	0.26	0.10	0.54
Fansi	FS-9	-0.78	0.07	0.19	0.04	0.26	0.03	0.31
Fansi	FS-10	-0.71	0.06	0.23	0.02	0.33	0.05	-
Fansi	FS-33	-0.74	0.07	0.21	0.05	0.30	0.05	0.27
Fansi	FS-33*			0.21	0.01	0.36	0.02	
Fansi	HHL-2	-0.69	0.08	0.21	0.01	0.30	0.01	0.33
Xiyang	FHS-1	-0.76	0.02	0.14	0.01	0.18	0.04	0.43
Xiyang	GB-2	-0.74	0.03	0.19	0.05	0.25	0.12	0.62
Xiyang	JD-1	-0.68	0.05	0.18	0.01	0.23	0.01	0.42
Xiyang	JX-1	-0.67	0.03	0.19	0.02	0.26	0.07	0.50
Xiyang	JX-3	-0.73	0.04	0.19	0.03	0.25	0.06	0.55
Xiyang	MAS-1	-0.75	0.05	0.19	0.05	0.26	0.04	0.56
Zuoquan	ZQ-1	-0.85	0.09	0.11	0.04	0.18	0.09	0.42
Zuoquan	ZQ-4	-0.77	0.06	0.14	0.02	0.21	0.05	0.25
Pingmingshan	13PMS1	-0.63	0.05	0.26	0.05	0.38	0.04	0.28
Pingmingshan	13PMS1*			0.27	0.02	0.37	0.06	
Pingmingshan	13PMS2	-0.65	0.07	0.25	0.05	0.38	0.04	0.38
Pingmingshan	13PMS2*	-0.60	0.02					
Pingmingshan	13PMS3	-0.67	0.03	0.23	0.01	0.39	0.11	0.39
Pingmingshan	13PMS4	-0.72	0.06	0.25	0.01	0.39	0.08	0.46
Pingmingshan	13PMS5	-0.61	0.08	0.26	0.03	0.38	0.02	0.42
Pingmingshan	13PMS6	-0.71	0.02	0.24	0.03	0.35	0.03	0.33
Pingmingshan	13PMS6*	-0.71	0.05					
Pingmingshan	13PMS7	-0.64	0.06	0.25	0.04	0.34	0.07	0.38
Pingmingshan	13PMS7*			0.25	0.05	0.36	0.05	
Anfengshan	13AFS9	-0.70	0.03	0.24	0.03	0.36	0.03	0.24
Anfengshan	13AFS10	-0.64	0.05	0.24	0.02	0.36	0.03	0.50
Fangshan	10FS6	-0.75	0.06	0.17	0.02	0.23	0.01	0.21
Fangshan	10FS9	-0.72	0.06	0.15	0.03	0.23	0.08	0.24
Fangshan	10FS10	-0.72	0.03	0.17	0.00	0.24	0.06	0.27
Fangshan	10FS10*	-0.77	0.04					
Longyou	10LYSK11	-0.71	0.02	0.19	0.01	0.25	0.03	0.47
Longyou	10LYSK13	-0.75	0.05	0.15	0.05	0.20	0.05	0.30

495 *duplicated analyses of sample dissolution, column chemistry and instrumental measurement

References

Ballhaus C. (1993) Redox states of lithospheric and asthenospheric upper mantle. Contrib. to Mineral. Petrol. 114, 331–348.

Berry A. J., Stewart G. A., O'Neill H. S. C., Mallmann G. and Mosselmans J. F. W. (2018) A re-assessment of the oxidation state of iron in MORB glasses. Earth Planet. Sci. Lett. 483, 114–123.

Bézos A. and Humler E. (2005) The Fe3+/ΣFe ratios of MORB glasses and their implications for mantle melting. Geochim. Cosmochim. Acta 69, 711–725.

Bigeleisen J. and Mayer M. G. (1947) Calculation of Equilibrium Constants for Isotopic Exchange Reactions. J. Chem. Phys. 15, 261–267.

Bougault H. and Hekinian R. (1974) Rift Valley in the Atlantic Ocean near 36°50′N: petrology and geochemistry of basaltic rocks. Earth Planet. Sci. Lett. 24, 249–261.

Braunger S., Marks M. A. W., Wenzel T., Chmyz L., Guitarrari Azzone R. and Markl G. (2020) Do carbonatites and alkaline rocks reflect variable redox conditions in their upper mantle source? Earth Planet. Sci. Lett. 533, 116041.

Brounce M., Cottrell E. and Kelley K. A. (2019) The redox budget of the Mariana subduction zone. Earth Planet. Sci. Lett. 528, 115859.

Brounce M. N., Kelley K. A. and Cottrell E. (2014) Variations in Fe3+/PFe of Mariana Arc Basalts and MantleWedge fO2. J. Petrol. 55, 2514–2536.

Carmichael I. S. E. (1991) The redox states of basic and silicic magmas: a reflection of their source regions? Contrib. to Mineral. Petrol. 106, 129–141.

Carmichael I. S. E. and Ghiorso M. S. (1986) Oxidation-reduction relations in basic magma: a case for homogeneous equilibria. Earth Planet. Sci. Lett. 78, 200–210.

Dasgupta R. and Hirschmann M. M. (2010) The deep carbon cycle and melting in Earth's interior. Earth Planet. Sci. Lett. 298, 1–13.

Ding X., Helz R. T., Qi Y. and Huang F. (2020) Vanadium isotope fractionation during differentiation of Kilauea Iki lava lake, Hawaii. Geochim. Cosmochim. Acta 289, 114–129.

Dong L. H., Wei W., Yu C. L., Hou Z. H., Zeng Z., Chen T. and Huang F. (2021) Determination of Vanadium Isotope Compositions in Carbonates Using an Fe Coprecipitation Method and MC-ICP-MS. Anal. Chem. 93, 7172–7179.

527 Evans K. A., Elburg M. A. and Kamenetsky V. S. (2012) Oxidation state of subarc mantle.
528 Geology 40, 783–786.

529 Greaney A. T., Rudnick R. L., Helz R. T., Gaschnig R. M., Piccoli P. M. and Ash R. D.
530 (2017) The behavior of chalcophile elements during magmatic differentiation as
531 observed in Kilauea Iki lava lake Hawaii. Geochim. Cosmochim. Acta 210, 71–96.

532 Guo P., Niu Y., Sun P., Gong H. and Wang X. (2020) Lithosphere thickness controls
533 continental basalt compositions: An illustration using Cenozoic basalts from
534 eastern China. Geology 48, 128–133.

535 Hart S. R. and Dunn T. (1993) Experimental cpx/melt partitioning of 24 trace elements.
536 Contrib. to Mineral. Petrol. 113, 1–8.

537 Hauri E. H., Wagner T. P. and Grove T. L. (1994) Experimental and natural partitioning of
538 Th, U, Pb and other trace elements between garnet, clinopyroxene and basaltic
539 melts. Chem. Geol. 117, 149–166.

540 He Y., Meng X., Ke S., Wu H., Zhu C., Teng F. Z., Hoefs J., Huang J., Yang W., Xu L.,
541 Hou Z., Ren Z. Y. and Li S. (2019) A nephelinitic component with unusual δ 56 Fe
542 in Cenozoic basalts from eastern China and its implications for deep oxygen cycle.
543 Earth Planet. Sci. Lett. 512, 175–183.

544 Higgins J. A. and Schrag D. P. (2010) Constraining magnesium cycling in marine
545 sediments using magnesium isotopes. Geochim. Cosmochim. Acta 74, 5039–5053.

546 Hofmann A. W., Jochum K. P., Seufert M. and White W. M. (1986) Nb and Pb in oceanic
547 basalts: new constraints on mantle evolution. Earth Planet. Sci. Lett. 79, 33–45.

548 Hong L., Xu Y. G., Zhang L., Wang Y. and Ma L. (2020) Recycled carbonate-induced
549 oxidization of the convective mantle beneath Jiaodong, Eastern China. Lithos 366–
550 367, 105544.

551 Huang F., Zhang Z., Lundstrom C. C. and Zhi X. (2011) Iron and magnesium isotopic
552 compositions of peridotite xenoliths from Eastern China. Geochim. Cosmochim.
553 Acta 75, 3318–3334.

554 Huang J., Li S. G., Xiao Y., Ke S., Li W. Y. and Tian Y. (2015) Origin of low δ26Mg
555 Cenozoic basalts from South China Block and their geodynamic implications.
556 Geochim. Cosmochim. Acta 164, 298–317.

557 Huang J. and Zhao D. (2006) High-resolution mantle tomography of China and
558 surrounding regions. J. Geophys. Res. Solid Earth 111, 1–21.

559 Jugo P. J. (2009) Sulfur content at sulfide saturation in oxidized magmas. Geology 37,
560 415–418.

561 Karner J. M., Sutton S. R., Papike J. J., Shearer C. K., Jones J. H. and Newville M. (2006)
562 Application of a new vanadium valence oxybarometer to basaltic glasses from the
563 Earth, Moon, and Mars. Am. Mineral. 91, 270–277.

564 Kilias S. P., Pozo M., Bustillo M., Stamatakis M. G. and Calvo J. P. (2006) Origin of the
565 Rubian carbonate-hosted magnesite deposit, Galicia, NW Spain: Mineralogical,
566 REE, fluid inclusion and isotope evidence. Miner. Depos. 41, 713–733.

567 Klein E. M. and Langmuir C. H. (1987) Glo bal Correlations of Ocean Ridge Basalt
568 Chemistry with Axial Depth and Crustal Thickness. J. Geophys. Res. Solid Earth
569 92, 8089–8115.

570 Laubier M., Grove T. L. and Langmuir C. H. (2014) Trace element mineral/melt
571 partitioning for basaltic and basaltic andesitic melts: An experimental and laser
572 ICP-MS study with application to the oxidation state of mantle source regions.
573 Earth Planet. Sci. Lett. 392, 265–278.

574 Li J. L., Klemd R., Gao J. and Meyer M. (2014) Compositional zoning in dolomite from
575 lawsonite-bearing eclogite (SW Tianshan, China): Evidence for prograde
576 metamorphism during subduction of oceanic crust. Am. Mineral. 99, 206–217.

577 Li S. G., Yang W., Ke S., Meng X., Tian H., Xu L., He Y., Huang J., Wang X. C., Xia Q.,
578 Sun W., Yang X., Ren Z. Y., Wei H., Liu Y., Meng F. and Yan J. (2017) Deep
579 carbon cycles constrained by a large-scale mantle Mg isotope anomaly in eastern
580 China. Natl. Sci. Rev. 4, 111–120.

581 Li Z. X. A. and Lee C. T. A. (2004) The constancy of upper mantle fO2 through time
582 inferred from V/Sc ratios in basalts. Earth Planet. Sci. Lett. 228, 483–493.

583 Liu S. A., Wang Z. Z., Li S. G., Huang J. and Yang W. (2016) Zinc isotope evidence for a
584 large-scale carbonated mantle beneath eastern China. Earth Planet. Sci. Lett. 444,
585 169–178.

586 Mallmann G. and O'Neill H. S. C. (2009) The crystal/melt partitioning of V during mantle
587 melting as a function of oxygen fugacity compared with some other elements (Al,
588 P, Ca, Sc, Ti, Cr, Fe, Ga, Y, Zr and Nb). J. Petrol. 50, 1765–1794.

589 McDonough W. F. and Sun S. s. (1995) The composition of the Earth. Chem. Geol. 120,
590 223–253.

de Moor J. M., Fischer T. P., Hilton D. R., Hauri E., Jaffe L. A. and Camacho J. T. (2005) Degassing at Anatahan volcano during the May 2003 eruption: Implications from petrology, ash leachates, and SO2 emissions. J. Volcanol. Geotherm. Res. 146, 117–138.

Moune S., Sigmarsson O., Thordarson T. and Gauthier P. J. (2007) Recent volatile evolution in the magmatic system of Hekla volcano, Iceland. Earth Planet. Sci. Lett. 255, 373–389.

Nielsen S. G., Bekaert D. V., Magna T., Mezger K. and Auro M. (2020) The vanadium isotope composition of Mars: implications for planetary differentiation in the early solar system. Geochemical Perspect. Lett. 15, 35–39.

Nielsen S. G., Prytulak J. and Halliday A. N. (2011) Determination of Precise and Accurate 51V/50V Isotope Ratios by MC-ICP-MS, Part 1: Chemical Separation of Vanadium and Mass Spectrometric Protocols. Geostand. Geoanalytical Res. 35, 293–306.

Novella D., Maclennan J., Shorttle O., Prytulak J. and Murton B. J. (2020) A multi-proxy investigation of mantle oxygen fugacity along the Reykjanes Ridge. Earth Planet. Sci. Lett. 531, 115973.

Pichat S., Douchet C. and Albarède F. (2003) Zinc isotope variations in deep-sea carbonates from the eastern equatorial Pacific over the last 175 ka. Earth Planet. Sci. Lett. 210, 167–178.

Prytulak J., Nielsen S. G. and Halliday A. N. (2011) Determination of Precise and Accurate 51V/50V Isotope Ratios by Multi-Collector ICP-MS, Part 2: Isotopic Composition of Six Reference Materials plus the Allende Chondrite and Verification Tests. Geostand. Geoanalytical Res. 35, 307–318.

Prytulak J., Nielsen S. G., Ionov D. A., Halliday A. N., Harvey J., Kelley K. A., Niu Y. L., Peate D. W., Shimizu K. and Sims K. W. W. (2013) The stable vanadium isotope composition of the mantle and mafic lavas. Earth Planet. Sci. Lett. 365, 177–189.

Prytulak J., Sossi P. A., Halliday A. N., Plank T., Savage P. S. and Woodhead J. D. (2017) Stable vanadium isotopes as a redox proxy in magmatic systems? Geochemical Perspect. Lett. 3, 75–84.

Qi Y. H., Gong Y. Z., Wu F., Lu Y., Cheng W., Huang F. and Yu H. M. (2022) Coupled variations in V-Fe abundances and isotope compositions in latosols: Implications for V mobilization during chemical weathering. Geochim. Cosmochim. Acta 320,

26–40.

Qi Y. H., Wu F., Ionov D. A., Puchtel I. S., Carlson R. W., Nicklas R. W., Yu H. M., Kang J. T., Li C. H. and Huang F. (2019) Vanadium isotope composition of the Bulk Silicate Earth: Constraints from peridotites and komatiites. Geochim. Cosmochim. Acta 259, 288–301.

Rohrbach A. and Schmidt M. W. (2011) Redox freezing and melting in the Earths deep mantle resulting from carbon-iron redox coupling. Nature 472, 209–214.

Le Roux V., Lee C. T. A. and Turner S. J. (2010) Zn/Fe systematics in mafic and ultramafic systems: Implications for detecting major element heterogeneities in the Earth's mantle. Geochim. Cosmochim. Acta 74, 2779–2796.

Rudnick R. L. and Gao S. (2003) Composition of the Continental Crust. In Treatise on Geochemistry Elsevier. pp. 1–64.

Schauble E. a (2004) Fractionation Theory to New Systems. Rev. Mineral. Geochemistry 55, 65–111.

Schuth S., Horn I., Brüske A., Wolff P. E. and Weyer S. (2017) First vanadium isotope analyses of V-rich minerals by femtosecond laser ablation and solution-nebulization MC-ICP-MS. Ore Geol. Rev. 81, 1271–1286.

Shorttle O., Moussallam Y., Hartley M. E., Maclennan J., Edmonds M. and Murton B. J. (2015) Fe-XANES analyses of Reykjanes Ridge basalts: Implications for oceanic crust's role in the solid Earth oxygen cycle. Earth Planet. Sci. Lett. 427, 272–285.

Sobolev A. V., Hofmann A. W., Kuzmin D. V., Yaxley G. M., Arndt N. T., Chung S.-L., Danyushevsky L. V., Elliott T., Frey F. A., Garcia M. O., Gurenko A. A., Kamenetsky V. S., Kerr A. C., Krivolutskaya N. A., Matvienkov V. V., Nikogosian I. K., Rocholl A., Sigurdsson I. A., Sushchevskaya N. M. and Teklay M. (2007) The Amount of Recycled Crust in Sources of Mantle-Derived Melts. Science (80-.). 316, 412–417.

Sutton S. R., Karner J., Papike J., Delaney J. S., Shearer C., Newville M., Eng P., Rivers M. and Dyar M. D. (2005) Vanadium K edge XANES of synthetic and natural basaltic glasses and application to microscale oxygen barometry. Geochim. Cosmochim. Acta 69, 2333–2348.

Tang Y. J., Zhang H. F. and Ying J. F. (2006) Asthenosphere-lithospheric mantle interaction in an extensional regime: Implication from the geochemistry of

656 Cenozoic basalts from Taihang Mountains, North China Craton. Chem. Geol. 233,
657 309–327.

658 Tao R. and Fei Y. Recycled calcium carbonate is an efficient oxidation agent under deep
659 upper mantle conditions. Commun. Earth Environ., 1–8.

660 Teng F. Z., Dauphas N., Huang S. and Marty B. (2013) Iron isotopic systematics of oceanic
661 basalts. Geochim. Cosmochim. Acta 107, 12–26.

662 Teng F. Z., Li W. Y., Ke S., Marty B., Dauphas N., Huang S., Wu F. Y. and Pourmand A.
663 (2010) Magnesium isotopic composition of the Earth and chondrites. Geochim.
664 Cosmochim. Acta 74, 4150–4166.

665 Thomson A. R., Walter M. J., Kohn S. C. and Brooker R. A. (2016) Slab melting as a
666 barrier to deep carbon subduction. Nature 529, 76–79.

667 Toplis M. J. and Corgne A. (2002) An experimental study of element partitioning between
668 magnetite, clinopyroxene and iron-bearing silicate liquids with particular emphasis
669 on vanadium. Contrib. to Mineral. Petrol. 144, 22–37.

670 Urey H. C. (1947) The Thermodynumic Properties of Isotopic Substances. J. Chem. Soc.,
671 562–581.

672 Wang Z.-Z., Liu S.-A., Chen L.-H., Li S.-G. and Zeng G. (2018) Compositional transition
673 in natural alkaline lavas through silica-undersaturated melt–lithosphere interaction.
674 Geology 46, 771–774.

675 Wang Z. Z., Liu S. A., Liu J., Huang J., Xiao Y., Chu Z. Y., Zhao X. M. and Tang L. (2017)
676 Zinc isotope fractionation during mantle melting and constraints on the Zn isotope
677 composition of Earth's upper mantle. Geochim. Cosmochim. Acta 198, 151–167.

678 Weyer S. and Ionov D. A. (2007) Partial melting and melt percolation in the mantle: The
679 message from Fe isotopes. Earth Planet. Sci. Lett. 259, 119–133.

680 Williams H. M., Peslier A. H., McCammon C., Halliday A. N., Levasseur S., Teutsch N.
681 and Burg J. P. (2005) Systematic iron isotope variations in mantle rocks and
682 minerals: The effects of partial melting and oxygen fugacity. Earth Planet. Sci. Lett.
683 235, 435–452.

684 Wu F., Owens J. D., Scholz F., Huang L., Li S., Riedinger N., Peterson L. C., German C.
685 R. and Nielsen S. G. (2020) Sedimentary vanadium isotope signatures in low
686 oxygen marine conditions. Geochim. Cosmochim. Acta 284, 134–155.

687 Wu F., Qi Y., Perfit M. R., Gao Y., Langmuir C. H., Wanless V. D., Yu H. and Huang F.

(2018) Vanadium isotope compositions of mid-ocean ridge lavas and altered oceanic crust. Earth Planet. Sci. Lett. 493, 128–139.

Wu F., Qi Y., Yu H., Tian S., Hou Z. and Huang F. (2016) Vanadium isotope measurement by MC-ICP-MS. Chem. Geol. 421, 17–25.

Wu F., Qin T., Li X., Liu Y., Huang J. H., Wu Z. and Huang F. (2015) First-principles investigation of vanadium isotope fractionation in solution and during adsorption. Earth Planet. Sci. Lett. 426, 216–224.

Xu Y. G., Ma J. L., Frey F. A., Feigenson M. D. and Liu J. F. (2005) Role of lithosphere-asthenosphere interaction in the genesis of Quaternary alkali and tholeiitic basalts from Datong, western North China Craton. Chem. Geol. 224, 247–271.

Yang W., Teng F. Z., Zhang H. F. and Li S. G. (2012) Magnesium isotopic systematics of continental basalts from the North China craton: Implications for tracing subducted carbonate in the mantle. Chem. Geol. 328, 185–194.

Zanetti A., Tiepolo M., Oberti R. and Vannucci R. (2004) Trace-element partitioning in olivine: Modelling of a complete data set from a synthetic hydrous basanite melt. Lithos 75, 39–54.

Zeng G., Chen L. H., Xu X. S., Jiang S. Y. and Hofmann A. W. (2010) Carbonated mantle sources for Cenozoic intra-plate alkaline basalts in Shandong, North China. Chem. Geol. 273, 35–45.

Zhou X. and Armstrong R. L. (1982) Trends in Chemistry and Strontium Isotopic Composition. 58, 301–329.